45th AIAA Aerospace Sciences Meeting
January 8–11, 2007
Reno, NV

AIAA 2007-0074

Dynamic Analysis of Atmospheric-Entry Probes and Capsules

Scott M. Murman*
ELORET Corp.
MS T27B
Moffett Field, CA 94035
smurman@mail.arc.nasa.gov

Michael J. Aftosmis†
NASA Ames Research Center
MS T27B
Moffett Field, CA 94035
maftosmis@mail.arc.nasa.gov

Abstract

A Computational Fluid Dynamics analysis of the dynamics of probe and capsule shapes at supersonic flight conditions is performed using an automated, inviscid Cartesian-mesh scheme. This analysis uses static and dynamic free-oscillation simulations to develop static and dynamic aerodynamic coefficients for three configurations: the Viking, Genesis, and Mars Exploration Rover capsules. These computed coefficients are compared against data reduced from ballistic-range free-flight testing. A comparison of data reduction methods for capsule shapes from computational simulations and range data is included. Free-flight simulations agree well with available flight data for both fully-coupled simulations and aerodynamic database fly-throughs based on the developed aerodynamic coefficients. A sensitivity analysis of the aerodynamic coefficients for trajectory simulations at constant altitude is included.

1 Introduction

Computational Fluid Dynamics (CFD) is a key technology in the design of NASA's Crew Exploration Vehicle (CEV) entry capsule. Atmospheric-entry capsule and probe shapes provide a challenge for numerical analysis due to the inevitable separation and bluff-body shedding over the aft end of the vehicle. This same unsteady physics creates difficulties for stability and control, as the pitch damping is adversely effected when it is most needed to damp the oscillations due to the unsteady wake. Further, accurately determining the pitch

*Senior Research Scientist, Member AIAA

†Aerospace Engineer, Senior Member AIAA

damping from experimental measurements for capsule and probe shapes has been a challenge dating to the Apollo and Viking programs (cf. [1–7]). This paper focuses on the use of high-fidelity CFD methods for probe and capsule dynamics in two areas: augmenting physical testing to calculate both the static and dynamic stability derivatives, and post-processing the results for stability and control analysis using aerodynamic database fly-throughs including dynamic effects.

An automated, Cartesian-mesh-based flow solver for static, unsteady, and dynamic moving-body simulations is utilized[8]. This solver has been validated for relevant unsteady physics including the calculation of dynamic stability derivatives using a forced-oscillation technique[9], and also against ballistic range trajectory data of foam debris as part of the NASA's Return-to-Flight (RTF) initiative[10, 11]. This work extends those previous studies by examining the static and dynamic predictions of the Cartesian solver for bluff-body flows against ballistic-range datasets for the Viking[4], Genesis[12], and Mars Exploration Rover (MER)[13] aeroshells (cf. Fig. 1). These cover a range of common configurations and provide an assessment of the sensitivity to shape changes. Further, a method of calculating damping derivatives using CFD simulations of free-oscillation and free-flight trajectories is presented and analyzed. The configurations investigated are all designed for a ballistic entry trajectory,* and tested with a static trim point of $\alpha = 0°$. While lifting trajectories are relevant for current designs such as the CEV or Mars Science Laboratory (MSL), non-lifting simulations are a necessary first step for CFD validation as free-flight range data for lifting shapes is limited due to testing constraints.

Due to the broad frequency spectra of capsule wake flowfields, high-fidelity CFD methods are not cost-effective for production design and optimization studies. Aerodynamic modeling, combined with 6-DOF trajectory calculations, provide an efficient and accurate alternative for rapidly analyzing large numbers of trajectories ($\mathcal{O}(1000)$ or greater). This aerodynamic database approach has been successfully applied using engineering aerodynamic methods to atmospheric-entry design studies[14–16]. Previous work by the authors demonstrated a prototype aerodynamic database tool based on high-fidelity static CFD results for design and optimization of stability and control methods[17]. This paper extends this work to the analysis of probe and capsule trajectories using aerodynamic database methods based on high-fidelity static and dynamic CFD data.

This paper covers the three main techniques of dynamic testing: forced-oscillation, free-oscillation, and free-flight. These are discussed specifically with the view of testing capsule shapes in the supersonic flight regime (roughly $1.5 \leq M_\infty \leq 4.0$). Dynamic stability in the supersonic regime is a critical factor for many mission profiles. Pitch damping coefficients from free-oscillation CFD simulations are compared against data reduced from ballistic-range testing. Sample free-flight fully-coupled trajectory calculations are also presented and compared against range data. Lastly, the predictive capability of the aerodynamic database developed for the MER capsule is examined, as well as the sensitivity of the aerodynamic database parameters.

*The Viking Entry Vehicle maintained a moderate L/D, however the model examined here is a sub-scale ballistic-range test model designed to trim at $\alpha = 0°$

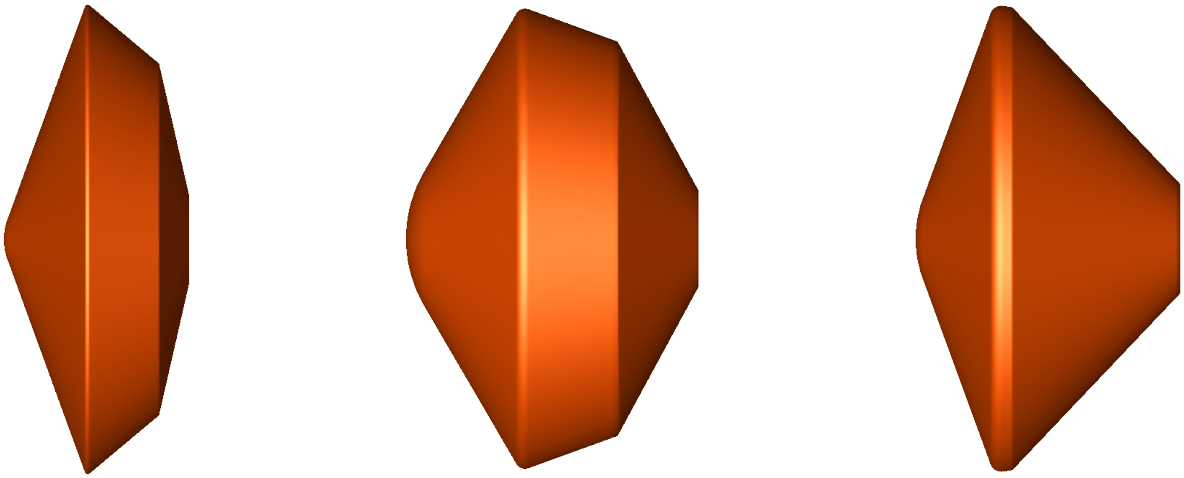

(a) Viking (b) Genesis (c) MER

Figure 1: Outer mold line of the capsule shapes examined. All shapes are idealized sub-scale models from ballistic range testing. Viking "model A" is described in [4]. Dimensions for the Genesis Sample Return Capsule (SRC) are found in [12], and the Mars Exploration Rover (MER) in [13]. MER uses inertial properties for the $x_{c.g.}/D = 0.27$ configuration.

2 Aerodynamic Modeling

Similar to experimental methods, a data reduction procedure is required to obtain dynamic damping coefficients from CFD moving-body simulations. If both the static and unsteady loads on the body are available, these can be used to determine the dynamic stability derivatives. In moving-body CFD simulations the time variation of the aerodynamic loads is computed, and it is recommended practice to first perform a static analysis of any configuration prior to beginning a dynamic analysis. A linear dynamic derivative can be calculated from

$$C_m(t) = C_m(\alpha) = C_{m_s}(\alpha) + \left(C_{m_q} + C_{m_{\dot{\alpha}}}\right) \frac{L}{4V_\infty} \left(q + \dot{\alpha}\right) \tag{1}$$

where C_{m_s} is the static contribution to the moment coefficient, and $C_{m_q} + C_{m_{\dot{\alpha}}}$ is the pitch damping sum. In forced- or free-oscillation simulations, more than one time level will map to a single angle of attack, and this procedure reduces to performing a linear regression for $C_m(\alpha)$ against the angular rate changes (cf. Fig. 2b). In the case of a linear aerodynamic response the calculation of the static loads can be foregone and obtained from the linear regression.

To demonstrate the method a Basic Finner missile configuration is used (cf. Fig. 2a). In the free-oscillation method, the missile is released from $\alpha = 20°$, and undergoes a damped oscillation through approximately 2-1/3 cycles (cf. Fig. 2b). Figure 2c contains the resulting damping derivatives compared to wind tunnel[18], range data[19], and computed values from the forced-oscillation method[9]. At the lower angles of attack the forced- and free-oscillation

methods agree well. The wind tunnel data suffers from sting effects below approximately $\alpha = 7°$[18], which are not present in the range data. At the higher angles of attack, the the free-oscillation simulation results and the tunnel data are in good agreeement. The results from the forced-oscillation simulations diverge slightly, likely due to high-angle-of-attack non-linear effects. It is not possible to fully account for these non-linear effects in a linear aerodynamic model such as Eqn. 1. Note that the free-oscillation method requires one unsteady computation, while the forced-oscillation simulation results use an unsteady small amplitude oscillation at each angle of attack.

Trajectory data for the current capsule ballistic range experiments are reduced to aerodynamic coefficients using the methods outlined by Chapman and Yates[5]. This 6-DOF software package is tailored specifically to bluff-body shapes, and infers aerodynamic coefficients from position and orientation data. From the observed data, the process can recommend either multi-fit linear or non-linear aerodynamic models. The non-linear pitching moment expansion from [5] is

$$\begin{aligned} C_m = C_{m_o} + \left[C_{m_\alpha} + C_{m_{\alpha,M_\infty}} \left(M_\infty - 1\right)\right] \sin\alpha + C_{m_{\alpha^3}} \sin^3\alpha \\ + \left[\left(C_{m_q} + C_{m_{\dot\alpha}}\right)_o + \left(C_{m_q} + C_{m_{\dot\alpha}}\right)_{\alpha^2} \sin^2\alpha\right] \frac{L}{4V_\infty} \left(q + \dot\alpha\right) \end{aligned} \tag{2}$$

with similar expressions for the remaining aerodynamic coefficients. Equation 2, along with multiple segment 6-DOF fitting procedures, provides a flexible method for evaluating capsule trajectory data. In order to utilize the non-linear aerodynamics model within an aerodynamics database, the same non-linear model must be implemented for the database fly-through.

This coupling between the data reduction and the aerodynamic database is present in the methodology for reducing CFD data to an aerodynamic model as well. Static coefficients from CFD simulations (C_{m_s} in Eqn. 1) are inherently a non-linear aerodynamic model, and contain no a priori assumptions about the form of the non-linearity, as opposed to Eqn. 2. The capsule simulations presented in Sec. 4 exhibit non-linear *dynamic* behavior as well. The assumed linear damping model, Eqn. 1, cannot accurately reproduce the dynamic trajectories. To correct this deficiency a dynamic "aerodynamic inertia" constant, $C_{m_{di}}$ is added to the assumed form

$$C_m = C_{m_s} + C_{m_{di}} + \left(C_{m_q} + C_{m_{\dot\alpha}}\right) \frac{L}{4V_\infty} \left(q + \dot\alpha\right) \tag{3}$$

A bluff body displaces a relatively large mass of fluid, and the inertia of this wake provides a lead or lag to the aerodynamic loading depending upon the flow conditions. It is noted that Eqn. 3 is not proposed as a general dynamic model for non-linear aerodynamics. The intent is to provide a useful approximation for reducing and analyzing the current CFD results, a consistent method for comparison against ballistic range data, and a method which can easily be implemented into standard aerodynamic database methods via augmentation of the static coefficients. In order to account for general non-linear aerodynamics for arbitrary configurations and flow conditions a formalized methodology is required, akin to that used in system identification[21]. This is beyond the scope of the current work, but provides an important topic for future research: develop a methodology for non-linear aerodynamics

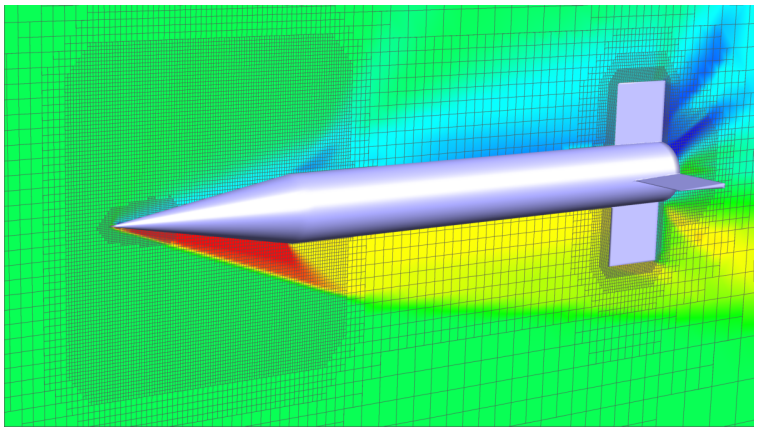

(a) Mesh and density contours ($M_\infty = 1.96$, $\alpha = 10°$).

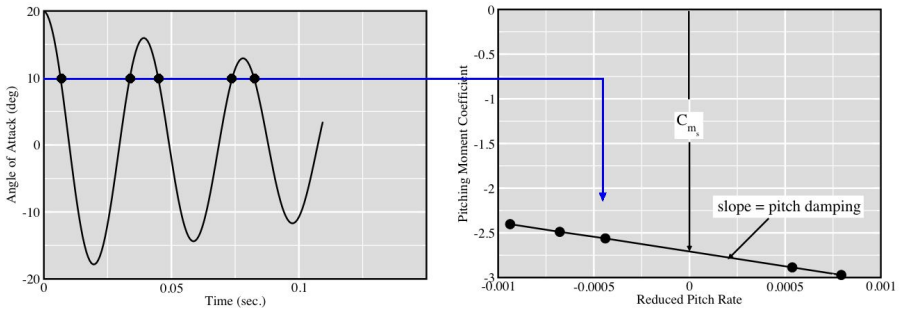

(b) Free-oscillation trajectory and data reduction of pitch damping sum.

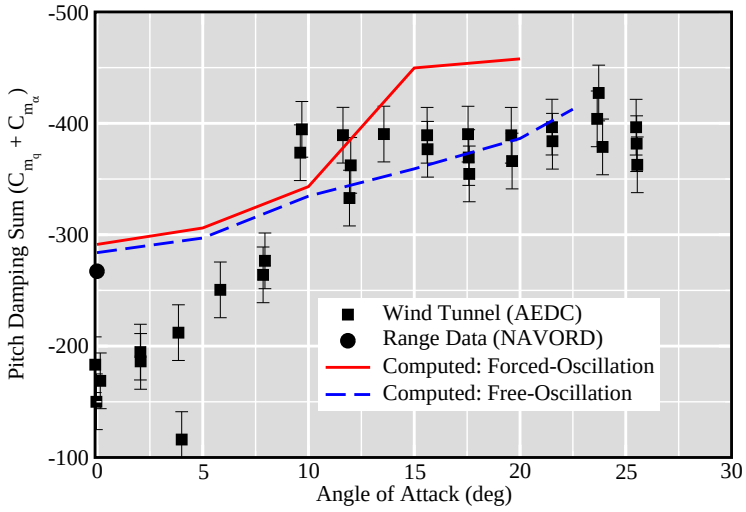

(c) Pitch Damping ($M_\infty = 1.96$).

Figure 2: Linear pitch damping data reduction for the Basic-Finner missile configuration. Wind tunnel data from [18]. Range data from [19].

to consistently handle experimental data reduction, CFD methods, and integration with aerodynamic database software.

The aerodynamic modeling for both the ballistic-range and CFD data reduction procedures represent nominal behavior. The CFD static coefficients are time averaged in cases with large unsteadiness, and the non-linear coefficients in Eqn. 2 remain constant. The unsteady 3-D wake causes the aerodynamic loads to vary about the nominal values. For example, the wake effect oscillates the pitching moment as much as the equivalent of $\pm 3^\circ$ angle of attack in the capsule simulations presented in the next sections. The importance of modeling this inherent uncertainty is investigated in the sensitivity analysis of Sec. 6.1.

3 Forced-oscillation

There are three main strategies for calculating dynamic derivatives: forced-oscillation, free-oscillation, and free-flight testing. Each of these techniques has strengths and weaknesses, and each can be simulated using numerical methods. However, for bluff-body shapes, such as probes and capsules, forced-oscillation testing can be difficult. The unsteady wake of an entry vehicle is both sensitive to perturbations and a strong factor in determining the vehicle pitch stiffness and damping coefficients. Figure 3 presents the sensitivity (adjoint field) of drag and pitching moment to axial momentum perturbations for the Mars Exploration Rover (MER) capsule from an adjoint solver[20]. Drag is primarily sensitive to changes ahead of the bow shock,* however the pitching moment is equally sensitive to changes ahead of the shock and in the aft wake. Further, these changes potentially counteract each other. This highlights the strongly non-linear behavior of the flowfield in the wake region. A forced-oscillation method adds energy to the flowfield, which further excites the wake region. This complex non-linear response can render simpler linear damping methods ineffective. To illustrate, Fig. 4 shows the computed response to a sinusoidal oscillation for the Genesis capsule shape. The amplification of the forcing energy into a high-frequency non-linear response is evident at Mach 1.5. The response to the same forcing oscillation at Mach 2.5, where the energy of the wake is more strongly damped, shows a linear response. Experimentally, many cycles of motion and a Fourier spectral analysis are required to estimate the damping properties at sensitive flow conditions (assuming sting effects can be minimized). Computing many cycles of motion is prohibitively expensive for production CFD computing, hence the forced-oscillation method is not preferred for blunt shapes with wake coupling.

4 Free-oscillation

As opposed to forced-oscillation testing, in free oscillations the inertia of the body removes energy from the flowfield, reducing the amplification of the wake response. In this method the body is perturbed away from a known static trim point, and then released. The model is "pinned", so that the resulting motion is 1-DOF in the pitch plane, and we have an angular

*The computed pressure contours are presented in Fig. 6.

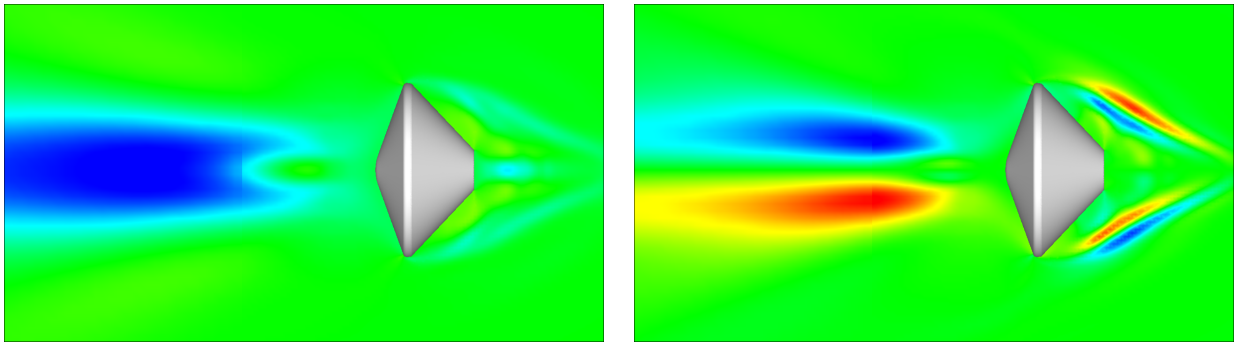

(a) Drag (b) Pitching Moment

Figure 3: Sensitivity of the aerodynamic load (adjoint field) to perturbations in axial momentum for the MER capsule[20]. The computed pressure contours are presented in Fig. 6. ($M_\infty = 2.5$, $\alpha = 0°$).

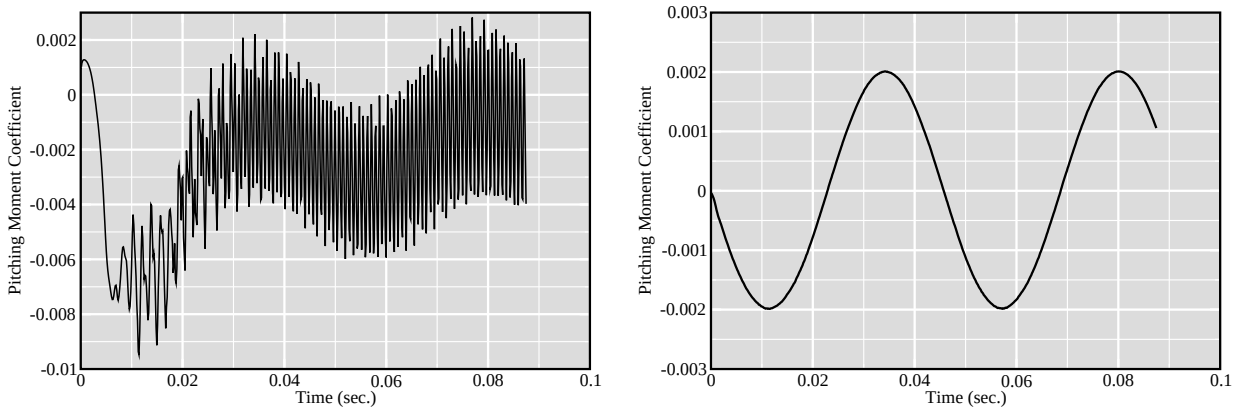

(a) $M_\infty = 1.5$ (b) $M_\infty = 2.5$

Figure 4: Computed pitching-moment response of the Genesis capsule 0.047-scale model to a 20Hz, $\pm 1.0°$ forced sinusoidal oscillation. ($\alpha = 0°$).

oscillation at constant Mach number (and dynamic pressure). Figure 5 demonstrates this technique for the same Genesis capsule shape and flow conditions shown in Fig. 4a. Two items are evident from the 1-DOF response in Fig. 5: the non-linear response is damped relative to the forced-oscillation results, and the capsule shape is unstable at these conditions.

Static and free-oscillation simulations were performed for the three configurations in Fig. 1 at supersonic conditions, and the aerodynamic coefficients compared against ballistic-range free-flight data reductions. For each shape a mesh convergence study determined the spatial resolution wherein the static coefficients converge. For inherently unsteady flows, the static coefficients were determined by averaging over a single period of the wake shedding (*sans* transient). The computational mesh obtained via the static convergence study was used throughout the dynamic calculations. The time resolution for the dynamic calculations resolves the wake shedding frequency using 50 timesteps per oscillation period with a second-order time-integration scheme. A sample cutting plane through the symmetry plane of the

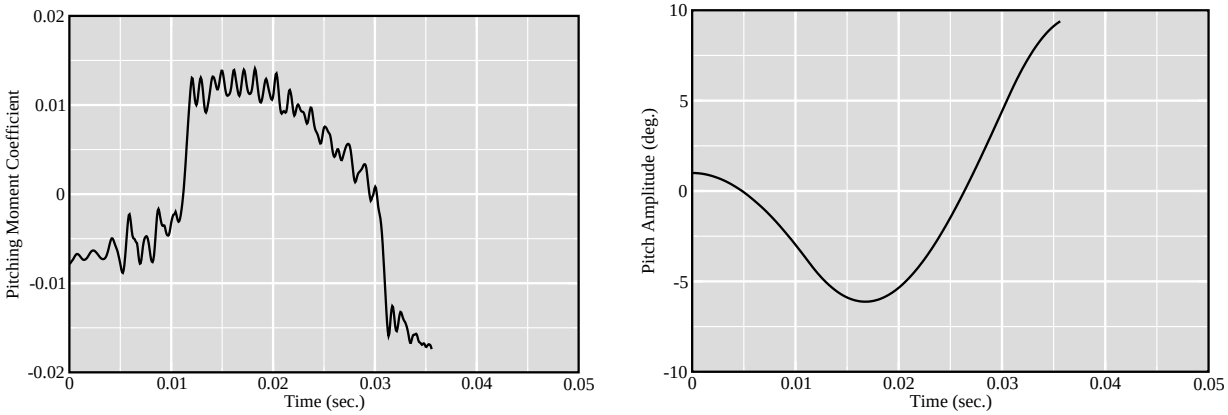

(a) Pitching Moment (b) Pitch Angle

Figure 5: Computed response of the Genesis capsule 0.047-scale model to 1° perturbation. ($M_\infty = 1.5$, $\alpha = 0°$).

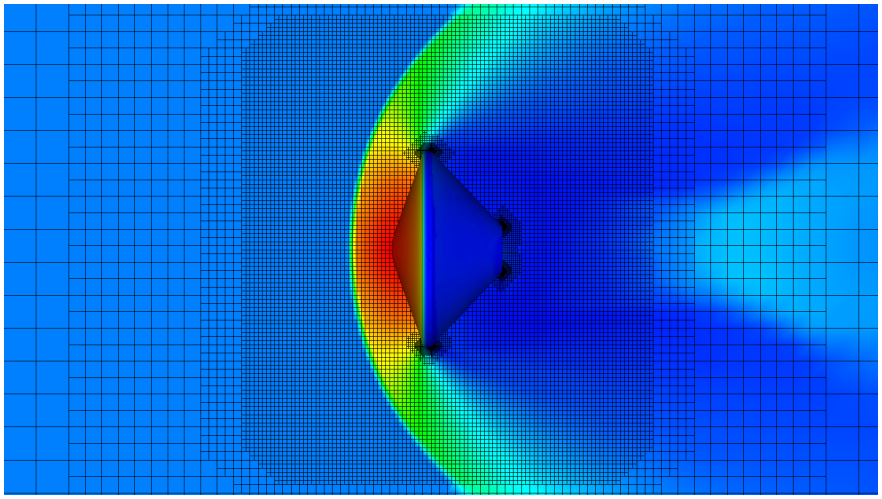

Figure 6: Computational mesh and pressure contours along the lateral symmetry plane for the MER capsule. ($M_\infty = 2.5$, $\alpha = 0°$).

computational mesh, along with computed pressure contours, for the MER configuration is shown in Fig. 6. A typical mesh contains around 1.5M cells, and requires roughly 100 Itanium2 cpu-hours to compute 2 oscillation cycles.

Figure 7 presents the linear pitch stiffness coefficient, C_{m_α}, from the static CFD simulations and the free-flight range data at the static trim point $\alpha = 0°$. The CFD simulations show that the pitching moment variation is actually non-linear for these configurations when $M_\infty \leq 2.5$ (approximately). Similar observations were determined from analysis of range data[5, 12, 13]. Because of the assumed form of the non-linearity in Eqn. 2, and the arbitrary non-linear form of the static computations, a reduced-order best-fit linear approximation was utilized in the comparisons. The static stiffness coefficient for the computations and the range

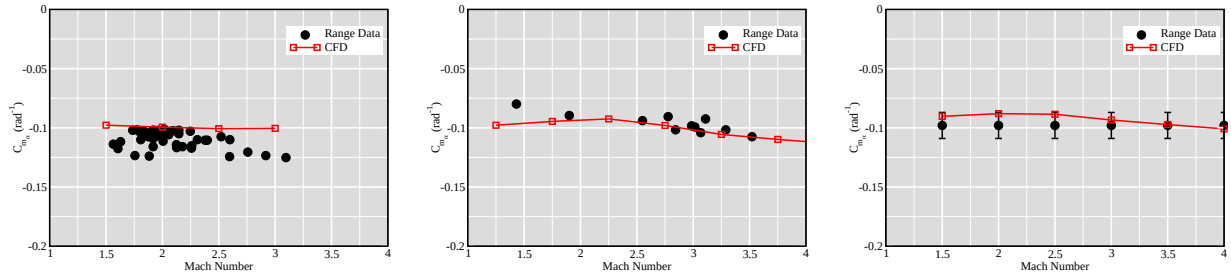

(a) Viking (b) Genesis (c) MER

Figure 7: Best linear fit for the trim pitch stiffness coefficient. Range data from [4, 12, 13]. MER data is reported as constant over the Mach number range.

data are in good agreement, and show little sensitivity to either configuration or angle of attack. The significance (or lack thereof) of the small variations in the static aerodynamic coefficients is investigated in Sec. 6.1.

Dynamic, free-oscillation simulations were performed for all three capsule configurations. Figure 8 shows the pitching moment variation with angle of attack for representative computations of the MER capsule. Also included is the computed static pitching moment variation for each Mach number. The arrows in the figure note the direction of increasing time. Several pieces of information can be gathered from the behavior in Fig. 8. The area within the regions of the hysteresis curve (counter-clockwise traversal for damping, clockwise destabilizing) indicate moderate damping at Mach 3.5, less damping at Mach 2.5, and instability at Mach 1.5. This behavior is confirmed in Fig. 9, which shows the time variation of angle of attack for the comparable simulations. Figure 8 also demonstrates non-linear dynamic behavior at Mach 1.5 and Mach 2.5.

The pitch damping sum computed from the CFD free-oscillation simulations using Eqn. 3 is plotted against linear-fit data for the Viking, Genesis, and MER configurations in Fig. 10. The trend in the comparisons shows the CFD aerodynamic coefficients predict greater damping at the higher Mach number, low angle-of-attack conditions than the reduced range data. Some of this increment is likely a result of the different aerodynamic model assumptions. The non-linear aerodynamic model applied to the range data also consistently contains a damping increment compared to the linear reductions (cf. Fig. 10 in [12] and Fig. 8 in [13]). The unstable flow conditions, $M_\infty = 1.5$, show relatively good agreement with the data, even though intuitively one would think these to be the most sensitive cases. There is consistently less damping at the statically-stable trim point, bounded by stable damping at higher angles of attack, which can lead to a limit cycle[6]. Further, as with the static stiffness coefficient, the damping parameters show relatively little sensitivity to shape changes within this family of similar configurations.

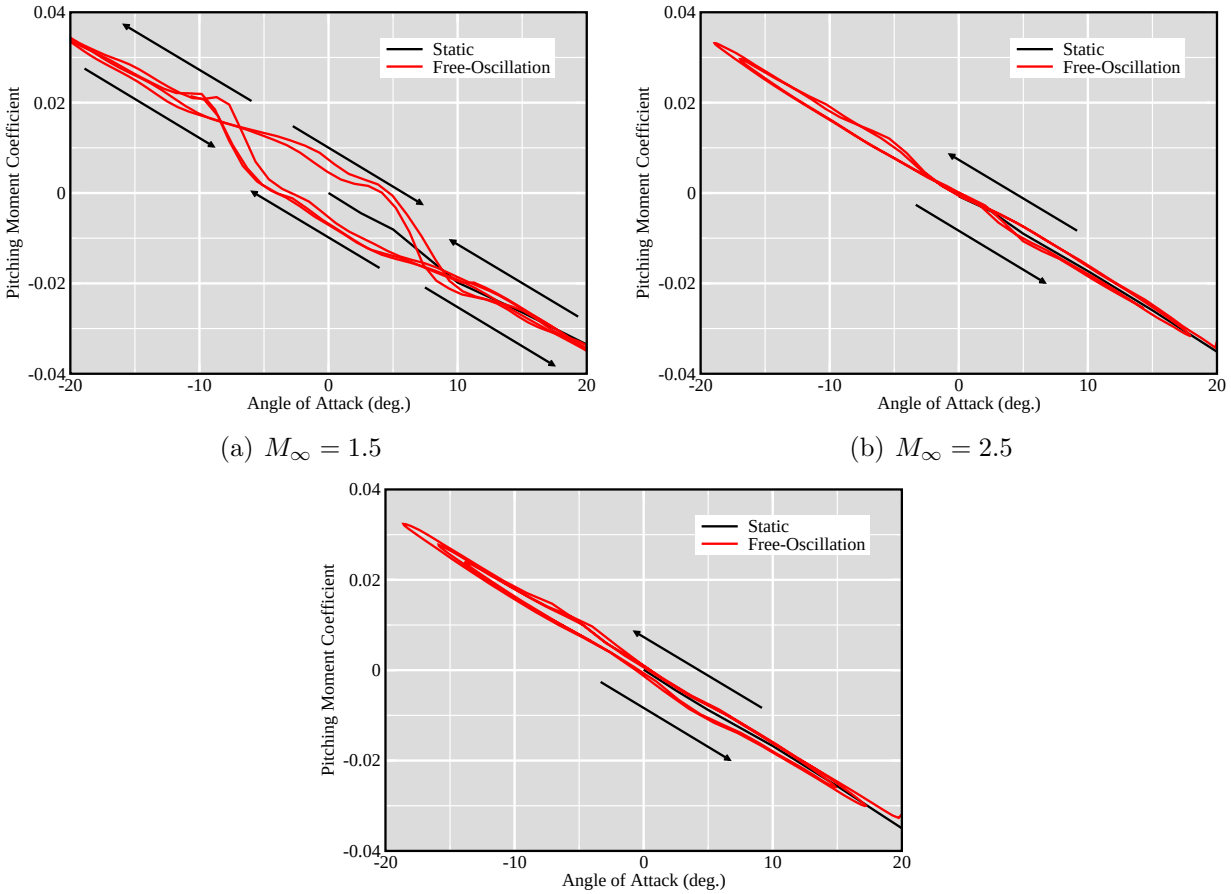

(a) $M_\infty = 1.5$ (b) $M_\infty = 2.5$

(c) $M_\infty = 3.5$

Figure 8: Variation of pitching moment with angle of attack from static and free-oscillation simulations of the MER capsule. Arrows indicate increasing time.

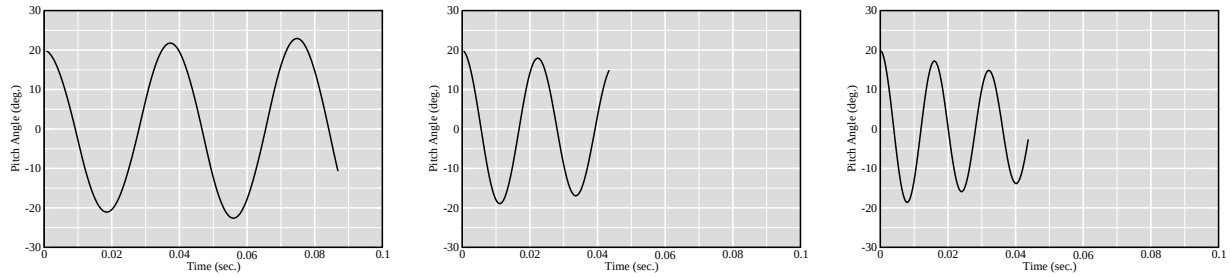

(a) $M_\infty = 1.5$ (b) $M_\infty = 2.5$ (c) $M_\infty = 3.5$

Figure 9: Temporal variation of pitch angle from free-oscillation simulations of the MER capsule.

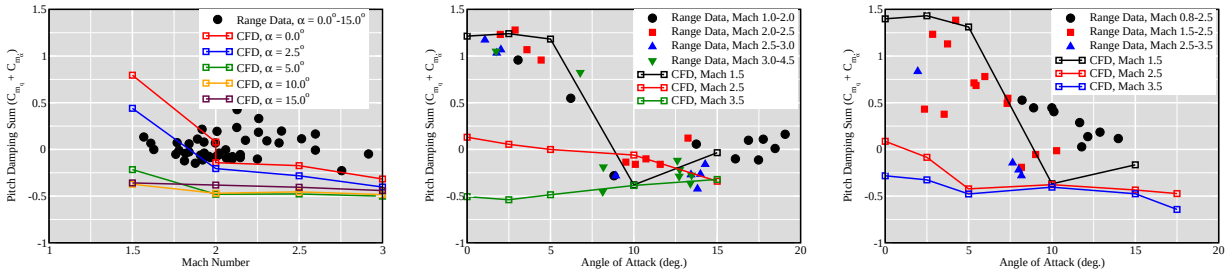

(a) Viking (b) Genesis (c) MER

Figure 10: Best linear fit for the pitch damping sum. Range data from [4, 12, 13].

5 Free-flight

The use of 1-DOF free-oscillation trajectories is a simplification of the general 6-DOF free-flight method. Free-flight trajectory calculations at constant altitude contain both Mach number and angle-of-attack variations. This poses a difficulty when encountering non-linear flight dynamics, as with the current capsule simulations. The approach for reducing CFD data outlined in Sec. 2 requires a minimum of two unsteady datapoints for each flight condition, and more complex methods could increase this requirement. Obtaining this redundant coverage of flight conditions with free-flight simulations is impractical. The experimental free-flight data reduction techniques avoid this complication by making a priori assumptions about the non-linear form of the coefficient variation with flight condition (cf. Eqn. 2).

Comparison of free-flight trajectory simulations against range data is compromised in the current work as details of the measured orientations and rates are not available in the literature. Without the ability to accurately match the initial conditions, comparable trajectories cannot be computed. Further, the uncertainty imposed on the aerodynamic loading due to the unsteady wake makes an exact comparison against measured trajectory data impractical. Qualitative comparisons of free-flight computed simulations against the non-linear reconstructed range data are provided to augment the discussion.

Figures 11 and 12 present comparisons of a CFD simulation and a non-linear reconstruction from range data for the Genesis capsule. As the body decelerates at constant altitude the dynamic pressure drops, causing the pitch amplitude to increase. This effect of decreasing dynamic pressure is counterbalanced (or augmented) by the pitch damping. Two variations of initial pitch amplitude are presented, and in both the initial flight Mach number is 4.5 which reduces to approximately 1.5 through the end of the trajectory. In both Figs. 11 and 12, the computed and reconstructed range trajectories are in good qualitative agreement. Beginning at approximately 140 meters downstream in the low-amplitude initial pitch rate data (Fig. 11), the velocity vector precesses about the body longitudinal axis as the capsule rotates, presenting a spiral trajectory. This is accompanied by a rapid growth in pitch amplitude as the damping reduces at the lower Mach number flight conditions. In Fig. 12, the higher angle-of-attack flight conditions maintain a greater damping, and the growth of the pitch amplitude is limited even at the lower velocities.

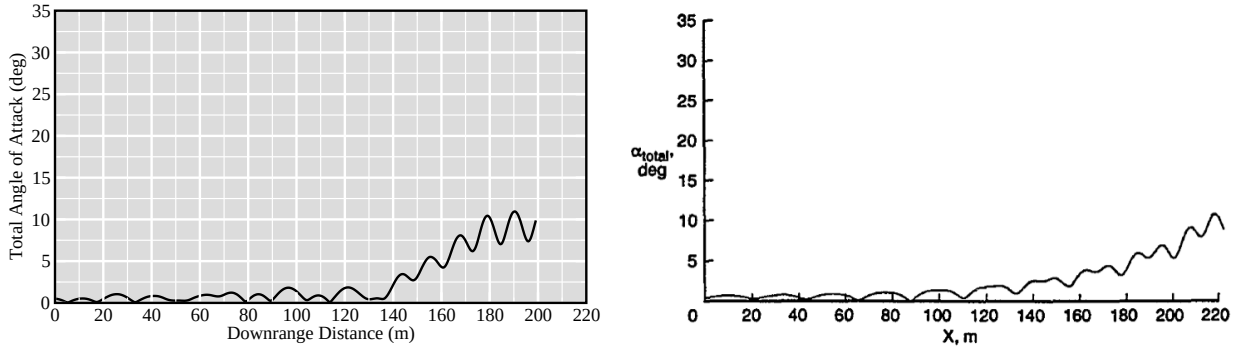

(a) Computed (b) Ballistic-range Reconstruction

Figure 11: Free-flight trajectories for the Genesis capsule. CFD simulation released from $M_\infty = 4.5$, $\alpha = 0.5°$. Fig. 11b taken from [12] with permission.

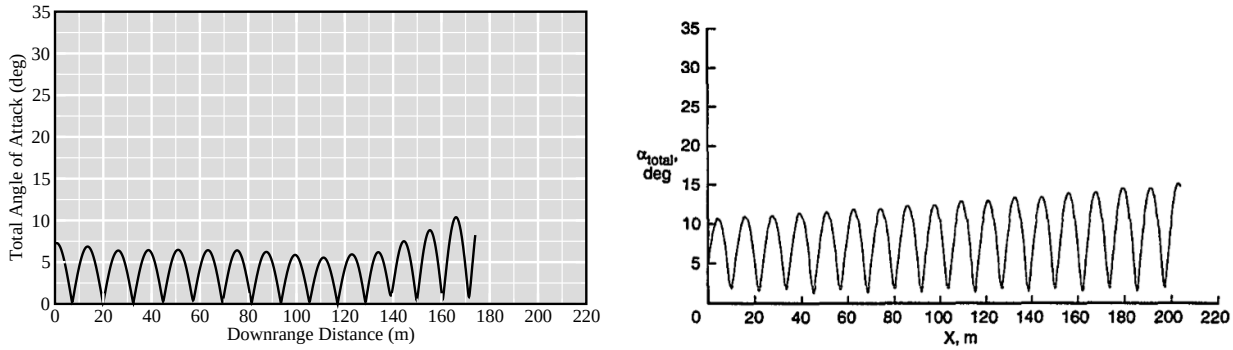

(a) Computed (b) Ballistic-range Reconstruction

Figure 12: Free-flight trajectories for the Genesis capsule. Time-dependent 6-DOF CFD simulations released from a $\pm 10°$ sinusoidal oscillation at $M_\infty = 4.5$. Fig. 12b taken from [12] with permission.

The qualitative changes in dynamic trajectory behavior with initial Mach number are compared against reconstructed range data for the MER capsule in Fig. 13. The reduction in damping with decreasing Mach number is evident in both the calculations and the range reconstructions. At Mach 2.0 and 2.5 a spiral trajectory develops as the velocity vector precesses about the body longitudinal axis. In both simulations and experiment, dynamic instability is apparent in the lower Mach number trajectories as the growth in mean total angle of attack is unchecked.

6 Aerodynamic Database Fly-through

Dynamic simulations are usually a means to an end, the end being an aerodynamic performance database which includes both static and dynamic effects. With an aerodynamic performance database in hand many applications become possible; developing control systems, shape or trajectory optimization, dispersion analysis, flight simulators, etc. An

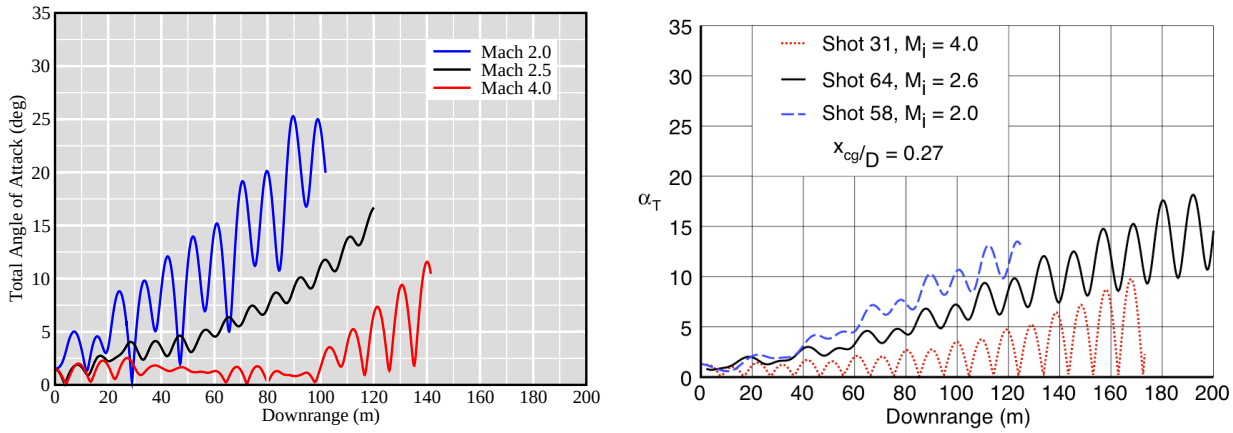

(a) Computed

(b) Ballistic-range Reconstruction

Figure 13: Free-flight trajectories for the MER capsule. Time-dependent 6-DOF CFD simulations released from $\alpha = 1.5°$. Fig. 13b taken from [13] with permission.

aerodynamic database fly-through based on static CFD data was presented in [17]. This application has been extended to include dynamic data.

Figure 14 reproduces the free-oscillation hysteresis behavior for the MER capsule from the fully-coupled CFD simulations (Fig. 8) using the non-linear CFD aerodynamic model (Eqn. 3), and an aerodynamic database fly-through. As expected, the results verify the aerodynamic model reproducing nominal trajectory data for the same flight conditions as the model was developed.

A further test is to examine free-flight trajectory results, comparing the fully-coupled CFD results with an aerodynamic database fly-through for comparable initial conditions. Figure 15 presents the orientation and dynamic increment, $C_m(t) - (C_{m_s} + C_{m_{di}})$, from a fully-coupled trajectory and from the aerodynamic database for the MER capsule when both are released at $M_\infty = 4$, $\alpha = 10°$. For reference, a dynamic increment of roughly 0.0017 corresponds to a change of one degree of angle of attack (cf. Fig. 7). Initially the aerodynamic model reconstructs the nominal behavior from the fully-coupled simulation, however the fully-coupled simulation contains an additional increment/decrement due to the oscillation of the wake. This effect is most pronounced when the body passes through the static trim point. This condition has both the largest unsteady effect in the static simulations, and the largest coupling effect due to the high oscillation rate. As the body decelerates the wake unsteadiness increases, and eventually the fully-coupled and database simulations start to slightly diverge. The fully-coupled simulation also demonstrates more coupling into the yaw axis due to the 3-D nature of the wake shedding.

As a cost comparison, the single fully-coupled 6-DOF trajectory in Fig. 15 requires approximately 3 times the cpu-time of a single free-oscillation computation due to the longer duration. The MER aerodynamic database was built using 6 free-oscillations simulations to cover the same increment of the trajectory. Hence, for the cost of two fully-coupled simulations the dynamic effects for the entire aerodynamic database were constructed. The cost of an actual aerodynamic database fly-through is less than a cpu-second.

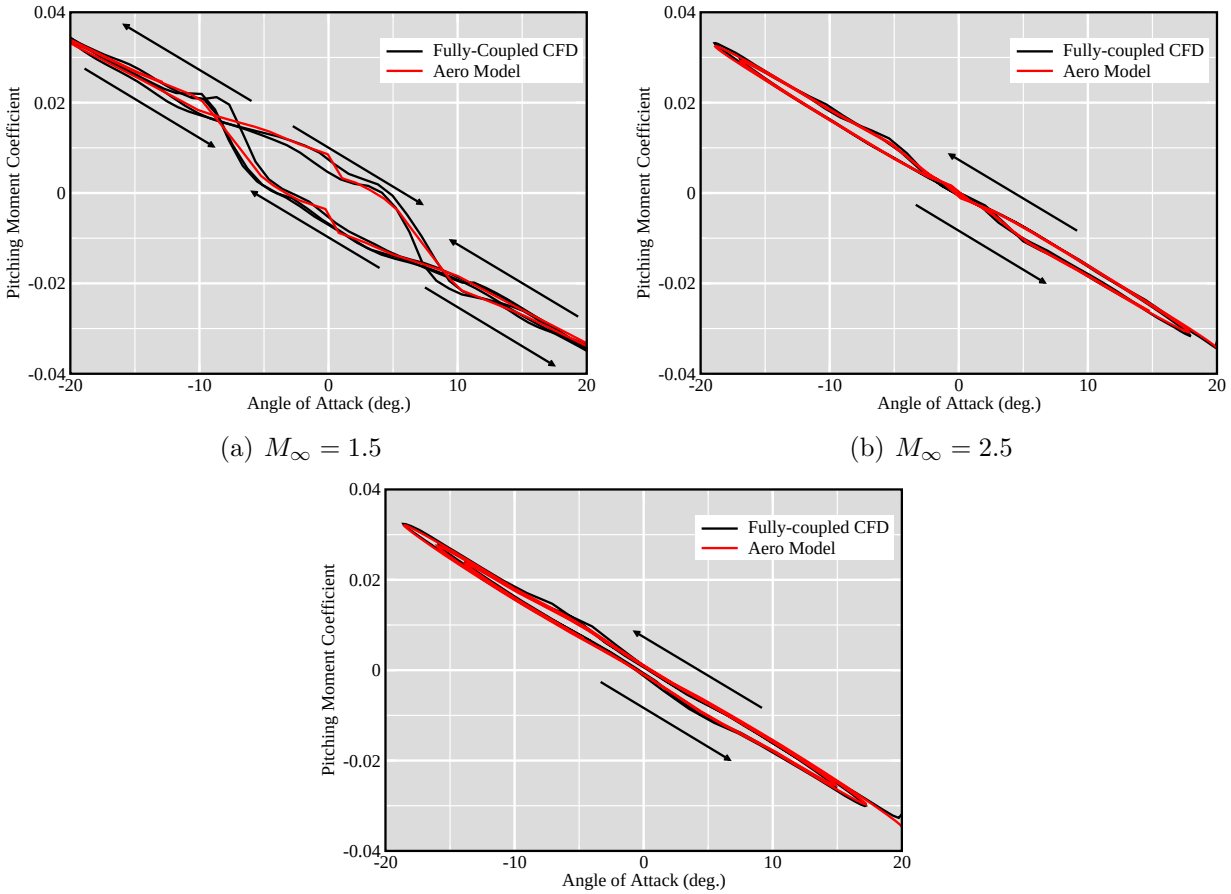

(a) $M_\infty = 1.5$

(b) $M_\infty = 2.5$

(c) $M_\infty = 3.5$

Figure 14: Variation of pitching moment with angle of attack from fully-coupled free-oscillation and aerodynamic database fly-through simulations of the MER capsule. Arrows indicate increasing time.

6.1 Sensitivity Assessment

Intuition indicates that the accuracy requirements for damping derivatives is lower than the requirements for static coefficients. A preliminary attempt to quantify the sensitivity to changes in aerodynamic parameters (uncertainty) for capsule trajectories is presented. Similar studies have been performed for full Entry, Decent, and Landing (EDL) scenarios using lower-fidelity aerodynamic models[14–16]. Here a constant altitude trajectory with fixed release conditions ($M_\infty = 4$, $\alpha = 10°$), and the aerodynamic database for the MER capsule, are used with varying aerodynamic coefficients. The maximum total angle of attack through Mach 1.5 is used as an objective function, and derivatives with respect to the changes in individual aerodynamic coefficient are calculated using finite differences. For an axisymmetric configuration the aerodynamic parameters of interest are C_A, C_N, C_m and $\left(C_{m_q} + C_{m_{\dot{\alpha}}}\right)$. These sensitivity derivatives at $\alpha = 10°$ and varying Mach number are presented in Fig. 16. This angle of attack has the greatest sensitivity for the current trajectory and objective function, and is representative of the general trends at different

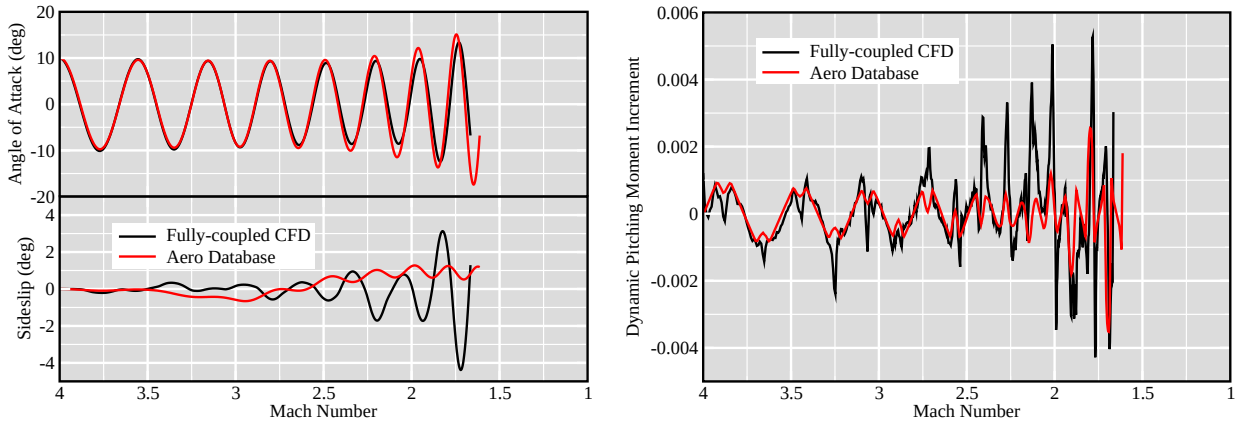

(a) Orientation

(b) Dynamic increment, $C_m(t) - (C_{m_s} + C_{m_{di}})$

Figure 15: Orientation and dynamic increment, $C_m(t) - (C_{m_s} + C_{m_{di}})$, from fully-coupled free-flight and aerodynamic database trajectories for the MER capsule. Released from $M_\infty = 4.0$, $\alpha = 10.0°$.

conditions. The greatest sensitivity is to changes in static pitching moment, by over an order of magnitude. Changes to the pitch damping sum show the least sensitivity. This is somewhat misleading for the current non-linear bluff-body flows however, as the aerodynamic inertia term ($C_{m_{di}}$ in Eqn. 3) represents an increment applied to the static pitching moment coefficient due to sensitivity to the unsteady wake. A full EDL analysis is left for future work, and will compare the uncertainty is aerodynamic coefficients to uncertainty in non-aerodynamic parameters such as entry orientation, atmospheric conditions, design tolerance, etc.

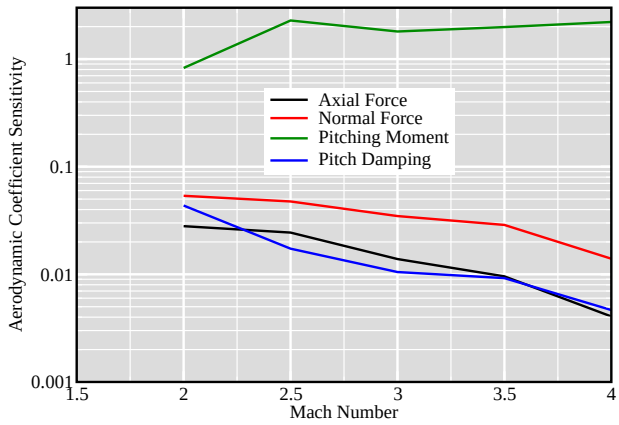

Figure 16: Sensitivity derivatives to changes in aerodynamic database parameters for a MER capsule trajectory released at $M_\infty = 4.0$, $\alpha = 10.0°$.

7 Summary

The non-linear coupling of the unsteady wake and the motion of bluff-body capsule shapes poses difficulties for dynamic analysis. High-fidelity CFD methods can play a role in obviating some of these difficulties due to their cost-effectiveness and detailed data acquisition. Free-oscillation and free-flight trajectory simulations were successfully used to analyze the damping characteristics of three separate zero-lift capsule shapes, and to develop a preliminary aerodynamic model which accurately reproduces the dynamic behavior. The use of automated, inviscid Cartesian-mesh software provides an efficient tool for preliminary design analysis, and a complement to Navier-Stokes methods or physical testing. The coupling of an automated fully-coupled CFD analysis with a general aerodynamic database enables the analysis of coefficient sensitivity to guide the overall design process, and the development of integrated system components or mission requirements.

A general method of parameter and system identification for these complex non-linear flows remains a challenge for future development. Integrating the data reduction and aerodynamic modeling between physical testing, CFD methods, and aerodynamic database analysis is an important step towards a coupled design process for bluff-body atmospheric-entry vehicles. Similarly, estimating and reproducing the inherent uncertainty due to the unsteady 3-D wake in both the data reduction and aerodynamic modeling phases is a challenge going forward.

Acknowledgments

The authors would like to thank Marian Nemec of ELORET Corp. for providing the adjoint field images for the MER capsule, as well as Neil Cheatwood and Mark Schoenenberger of NASA Langley Research Center for permission to reproduce figures from their respective publications. Scott Murman was supported by NASA Ames Research Center (contract NNA06BC19C) during this work.

References

[1] Redd, B., Olsen, D. M., and Burton, R. L., "Relationship Between the Aerodynamic Damping Derivatives Measured as a Function of Instantaneous Angular Displacement and the Aerodynamic Damping Derivatives Measured as a Function of Oscillation Amplitude," NASA TN D-2855, June 1965.

[2] Moseley, Jr., W.C., Graham, R.E., Hughes, J.E., "Aerodynamic Stability Characteristics of the Apollo Command Module," NASA TN D-4688, August 1968.

[3] Steinberg, S., Uselton, B.L., and Siemers, III, P.M., "Viking Pitch Damping Derivatives as Influenced by Support Interference and Test Techniques," *Journal of Spacecraft and Rockets*, 10(7):443–449, July 1973.

[4] Sammonds, R.I. and Kruse, R. L., "Viking Entry Vehicle Aerodynamics at M = 2 in Air and Some Preliminary Test Data for Flight in CO_2 at M = 11," NASA TN D-7974, June 1975.

[5] Chapman, G.T. and Yates, L.A., "Dynamics of Planetary Probes: Design and Testing Issues," AIAA Paper 1998-0797, January 1998.

[6] Chapman, G.T. and Yates, L.A., "Limit Cycle Analysis of Planetary Probes," AIAA Paper 1999-0496, January 1999.

[7] Winchenbach, G.L., Chapman, G.T., Hathaway, W., Ramsey, A., and Berner, C., "Dynamic Stability of Blunt Atmospheric Entry Configurations," *Journal of Spacecraft and Rockets*, 39(1):49–55, January 2002.

[8] Murman, S.M., Aftosmis, M.J., and Berger, M.J., "Implicit Approaches for Moving Boundaries in a 3-D Cartesian Method," AIAA Paper 2003-1119, January 2003.

[9] Murman, S.M., "A Reduced-Frequency Approach for Calculating Dynamic Derivatives," AIAA Paper 2005-0840, January 2005.

[10] Murman, S.M., Aftosmis, M.J., and Rogers, S.E., "Characterization of Space Shuttle Ascent Debris Aerodynamics Using CFD Methods," AIAA Paper 2005-1223, January 2005.

[11] Brown, J. D., Bogdanoff, D. W., Yates, L. A., Wilder, M. C., and Murman, S.M., "Complex-Trajectory Aerodynamics Data for Code Validation from a New Free-Flight Facility," AIAA Paper 2006-0662, January 2006.

[12] Cheatwood, F.M., Winchenbach, G.L., Hathaway, W., and Chapman, G., "Dynamic Stability Testing of the Genesis Sample Return Capsule," AIAA Paper 2000-1009, January 2000.

[13] Schoenenberger, M., Hathaway, W., Yates, L., and Desai, P., "Ballistic Range Testing of the Mars Exploration Rover Entry Capsule," AIAA Paper 2005-0055, January 2005.

[14] Braun, R.D., Powell, R.W., Engelund, W.C., Gnoffo, P.A., Weilmuenster, K.J., and Mitcheltree, R.A., "Mars Pathfinder Six-Degree-of-Freedom Entry Analysis," *Journal of Spacecraft and Rockets*, 32(6):993–1000, November 1995.

[15] Desai, P.N., Mitcheltree, R.A., and Cheatwood, F.M., "Entry Dispersion Analysis for the Stardust Comet Sample Return Capsule," *Journal of Spacecraft and Rockets*, 36(3): 463–469, May 1999.

[16] Desai, P.N. and Cheatwood, F.M., "Entry Dispersion Analysis for the Genesis Sample Return Capsule," *Journal of Spacecraft and Rockets*, 38(3):345–350, May 2001.

[17] Murman, S.M., Aftosmis, M.J., and Nemec, M., "Automated Parameter Studies Using a Cartesian Method," AIAA Paper 2004-5076, August 2004.

[18] Uselton, B.L. and Uselton, J.C., "Test Mechanism for Measuring Pitch Damping Derivatives of Missile Configurations at High Angles of Attack," AEDC Technical Report AEDC-TR-75-43, May 1975.

[19] Shantz, I. and Graves, R.T., "Dynamic and Static Stability Measurements of the Basic Finner at Supersonic Speeds," NAVORD Report 4516, September 1960.

[20] Nemec, M., Aftosmis, M. J., Murman, S. M., and Pulliam, T. H., "Adjoint Formulation for an Embedded-Boundary Cartesian Method," AIAA Paper 2005-0877, January 2005.

[21] Morelli, E. A. and Klein, V., "Application of System Identification to Aircraft at NASA Langley Research Center," *Journal of Aircraft*, 42(1):12–25, January 2005.